Biomaterials 32 (2011) 4118–4129

Contents lists available at ScienceDirect

Biomaterials

journal homepage: www.elsevier.com/locate/biomaterials

N-acetylgalactosamine-functionalized dendrimers as hepatic cancer cell-targeted carriers

Scott H. Medina [a], Venkatesh Tekumalla [a], Maxim V. Chevliakov [a], Donna S. Shewach [b], William D. Ensminger [c], Mohamed E.H. El-Sayed [a,d,*]

[a] University of Michigan, Department of Biomedical Engineering, Cellular Engineering and Nano-Therapeutics Laboratory, 1101 Beal Avenue, Ann Arbor, MI 48109, USA
[b] University of Michigan, Department of Pharmacology, 1150 W. Medical Center Drive, Ann Arbor, MI 48109, USA
[c] University of Michigan, Department of Internal Medicine, 1150 W. Medical Center Drive, Ann Arbor, MI 48109, USA
[d] University of Michigan, Macromolecular Science and Engineering Program, Ann Arbor, MI 48109, USA

ARTICLE INFO

Article history:
Received 15 November 2010
Accepted 27 November 2010
Available online 22 March 2011

Keywords:
Nanoparticle
Dendrimers
Drug delivery
Flow cytometry
Hepatocyte

ABSTRACT

There is an urgent need for novel polymeric carriers that can selectively deliver a large dose of chemotherapeutic agents into hepatic cancer cells to achieve high therapeutic activity with minimal systemic side effects. PAMAM dendrimers are characterized by a unique branching architecture and a large number of chemical surface groups suitable for coupling of chemotherapeutic agents. In this article, we report the coupling of *N*-acetylgalactosamine (NAcGal) to generation 5 (G5) of poly(amidoamine) (PAMAM-NH_2) dendrimers via peptide and thiourea linkages to prepare NAcGal-targeted carriers used for targeted delivery of chemotherapeutic agents into hepatic cancer cells. We describe the uptake of NAcGal-targeted and non-targeted G5 dendrimers into hepatic cancer cells (HepG2) as a function of G5 concentration and incubation time. We examine the contribution of the asialoglycoprotein receptor (ASGPR) to the internalization of NAcGal-targeted dendrimers into hepatic cancer cells through a competitive inhibition assay. Our results show that uptake of NAcGal-targeted G5 dendrimers into hepatic cancer cells occurs via ASGPR-mediated endocytosis. Internalization of these targeted carriers increased with the increase in G5 concentration and incubation time following Michaelis–Menten kinetics characteristic of receptor-mediated endocytosis. These results collectively indicate that G5-NAcGal conjugates function as targeted carriers for selective delivery of chemotherapeutic agents into hepatic cancer cells.

1. Introduction

Tomalia and co-workers first reported the synthesis of poly(amidoamine) (PAMAM) dendrimers as a new class of branched, water-soluble polymers in 1985 [1]. PAMAM dendrimers are characterized by a unique tree-like branching architecture and exhibit a characteristic increase in size, molecular weight, and number of surface functional groups with the increase in generation number [2]. Aqueous solubility, monodispersity, and large number of surface groups of PAMAM dendrimers available for conjugation of therapeutic molecules, targeting ligands, and imaging agents make these polymers ideal carriers for both diagnostic and therapeutic applications [2–6]. For example, PAMAM dendrimers have been used as gene [7–9] and anticancer drug carriers [2,3,10] that may display an antibody for cell or tissue targeting [11,12].

In this article, we report the synthesis of PAMAM-sugar conjugates that can target hepatic cancer cells for selective drug delivery. We selected generation 5 (G5) of PAMAM-NH_2 dendrimers as a carrier due to the large number of primary amine surface groups that can be used for attachment of drug molecules, imaging agents, and targeting ligands. To develop a carrier that can selectively target hepatic cancer, we utilized G5 dendrimers with a diaminobutane (DAB) core to construct the *N*-acetylgalactosamine-functionalized carriers due to their intrinsic ability to accumulate in the liver compared to dendrimers with ethylenediamine cores (EDA) [5,6]. In addition, G5 dendrimers with a DAB core proved to preferentially extravasate across the leaky tumor vasculature while exhibiting insignificant extravasation across normal blood vessels [13], which allows effective *in vivo* targeting of these carriers to tumor tissue [12,14–17]. We envision that conjugation of *N*-acetylgalactosamine (NAcGal) molecules to G5 dendrimers will provide an additional

* Corresponding author. University of Michigan, Department of Biomedical Engineering, 1101 Beal Avenue, Lurie Biomedical Engineering Building, Room 2150, Ann Arbor, MI 48109, USA. Tel.: +1 (734) 615 9404; fax: +1 (734) 647 4834.
E-mail address: meslayed@umich.edu (M.E.H. El-Sayed).
URL: http://www.bme.umich.edu/centlab.php

0142-9612/$ – see front matter © 2011 Elsevier Ltd. All rights reserved.
doi:10.1016/j.biomaterials.2010.11.068

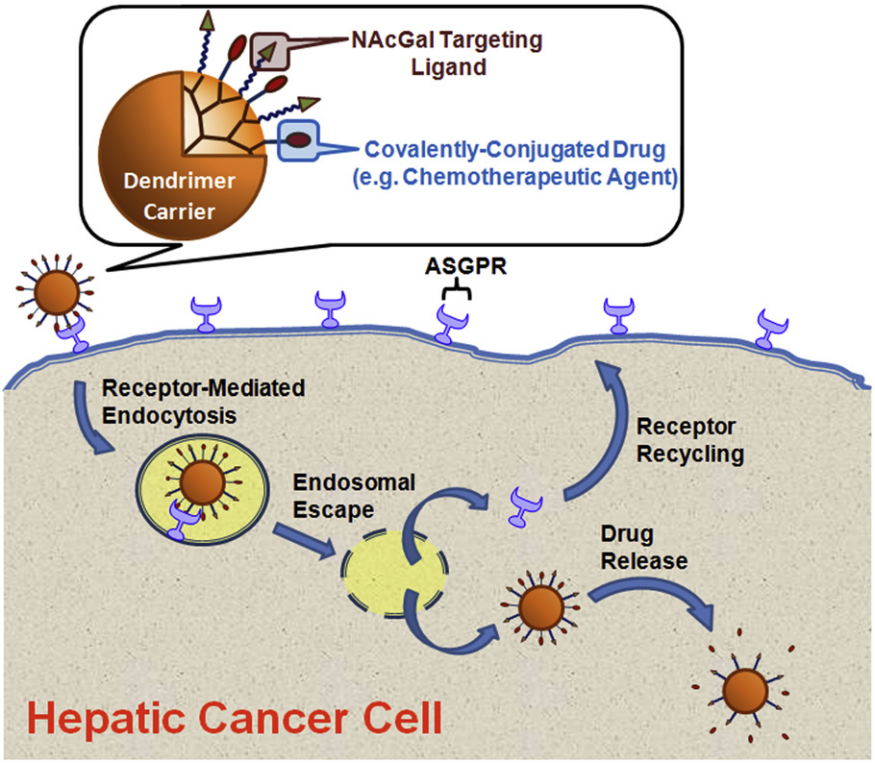

Fig. 1. A schematic drawing showing the composition of a drug-loaded G5-NAcGal conjugate binding to the ASGPR expressed on the surface of hepatic cancer cells (e.g. HepG2), which triggers receptor-mediated endocytosis of these G5-NAcGal conjugates followed by endosomal escape and release of the therapeutic cargo into the cytoplasm while the ASGPR recycles back to the cell surface.

strategy to increase their accumulation and retention in hepatic tumor tissue and warrant their use as carriers for targeted delivery of chemotherapeutic agents.

We report the conjugation of *N*-acetylgalactosamine (NAcGal) sugar molecules to the primary amine surface groups of G5-$(NH_2)_{128}$ dendrimers via peptide and thiourea linkages to prepare G5-NAcGal conjugates with various sugar density. These G5-NAcGal conjugates are designed to achieve selective binding to the asialoglycoprotein receptor (ASGPR) that is highly expressed on the surface of hepatic cancer cells [18], which will trigger their receptor-mediated endocytosis into hepatic cancer cells (Fig. 1). We evaluated the effect of surface charge, concentration, incubation time, number of conjugated NAcGal molecules, and linkage chemistry on the uptake of G5-NAcGal conjugates into human hepatic cancer cells (HepG2). Selectivity of G5-NAcGal conjugates toward hepatic cancer cells and the contribution of the ASGPR to conjugate's internalization was also evaluated using a competitive inhibition assay and assessing conjugates' uptake into MCF-7 breast cancer cells, which lack the ASGPR. MCF-7 breast cancer cells were selected for this comparison due to their high endocytic capacity and their reported use as a control cell line to test selectivity of galactosylated carriers toward the ASGPR [19].

2. Materials and methods

2.1. Materials

G5-$(NH_2)_{128}$ PAMAM dendrimers with DAB core, *N*-acetylgalactosamine, fluorescein isothiocyanate (Fl), and bovine insulin were purchased from Sigma-Aldrich Inc. (St. Louis, MO). Minimum essential medium (MEM), OPTI-MEM reduced serum medium, fetal bovine serum (FBS), 0.25% trypsin/0.20% ethylene diamine teraacetic acid (EDTA), phosphate buffered saline (PBS), penicillin/streptomycin/amphotericin, sodium pyruvate, and non-essential amino acid solutions were purchased from Invitrogen Corporation (Carlsbad, CA). Cytotoxicity Detection Kit (Lactate Dehydrogenase; LDH) was purchased from Roche Diagnostics Corporation (Indianapolis, IN). T-75 flasks, Costar 24-well plates, and cell culture supplies were purchased from Corning Inc. (Corning, NY). HepG2 and MCF-7 cells were generous gifts from Dr. Donna Shewach and Dr. Sofia Merajver, respectively.

2.2. Synthesis of fluorescently-labeled G5-NAcGal conjugates via peptide linkages

2.2.1. Synthesis of 3-(carbo-t-butoxymethyl)-2-(acetylamino)-2-deoxy-D-galactopyranoside (*1*)

NAcGal (486 mg, 2.2 mmol) was dissolved in 10 ml of dimethylformamide (DMF) and NaH (88 mg, 2.2 mmol) was added as a solid followed by the addition of tert-butyl bromoacetate (429.1 mg, 2.2 mmol) in 2 ml of DMF. After stirring at room temperature for 72 h, DMF was removed under reduced pressure and the reaction mixture was purified on a silica gel column using a consecutive eluent system of CH_2Cl_2 (100%), CH_2Cl_2:methanol (15:1), CH_2Cl_2:methanol (10:1) and finally CH_2Cl_2:methanol (8:1) to produce 400 mg (54% yield) of product **1** as a white solid. ^{1}H NMR of compound **1** in CD_3OD (400 MHz Varian, Palo Alto, CA) shows δ 4.92 (d, $J = 4.8$ Hz, 1H), 4.36 (dd, $J_1 = 9.2$ Hz, $J_2 = 4.8$ Hz, 1H), 4.26 (dd, $J_1 = 9.2$ Hz, $J_2 = 7.2$ Hz, 1H), 4.15 (s, 2H), 3.82 (dd, $J_1 = 7.6$ Hz, $J_2 = 3.6$ Hz, 1H), 3.62–3.52 (m, 3H), 3.29 (m, 1H), 2.00 (s, 3H), 1.45 (s, 9H); ESI Mass of compound **1** is 358 $[M + Na]^+$.

2.2.2. Synthesis of 3-(carbo-t-butoxymethyl)-2-(acetylamino)-2-deoxy-D-galactopyranoside-3,4,6-triacetate (*2*)

Excess of pyridine (0.145 ml, 1.79 mmol) and acetic anhydride (0.34 ml, 3.58 mmol) were added to compound **1** (67 mg, 0.179 mmol) dissolved in 2 ml of anhydrous dichloromethane and the reaction mixture was stirred at room temperature for 16 h. The reaction mixture was diluted with 50 ml CH_2Cl_2, washed twice with 20 ml of 0.1 N HCl followed by an additional wash with 20 ml DI water. The organic layer was dried over $MgSO_4$ and concentrated providing 57 mg (69% yield) of product **2** as a colorless oil, which was used as the crude product in the next step without any further purification. ^{1}H NMR of compound **2** in $CDCl_3$ (500 MHz Varian, Palo Alto, CA) shows δ 6.48 (d, $J = 9.0$ Hz, 1H), 5.36 (t, $J = 7.0$ Hz, 1H), 5.17 (q, $J = 5.5$ Hz, 1H), 4.97 (m, 1H), 4.66 (m, 1H), 4.23 (dd, $J_1 = 12.0$ Hz, $J_2 = 4.5$ Hz, 1H), 4.17 (m, 2H), 4.10 (dd, $J_1 = 12.0$ Hz, $J_2 = 6.0$ Hz, 1H), 3.98 (d, $J = 16.5$ Hz, 1H), 2.08 (s, 3H), 2,04 (s, 3H), 2.03 (s, 3H), 1.97 (s, 3H), 1.46 (s, 9H); ESI Mass of compound **2** is 462 $[M + H]^+$.

2.2.3. Synthesis of 3-(carboxymethyl)-2-(acetylamino)-2-deoxy-D-galactopyranoside-3,4,6-triacetate (*3*)

Trifluoroacetic acid (1 ml) was added to a solution of compound **2** (55 mg, 0.119 mmol) dissolved in 2 ml of CH_2Cl_2 and the reaction mixture was stirred at room

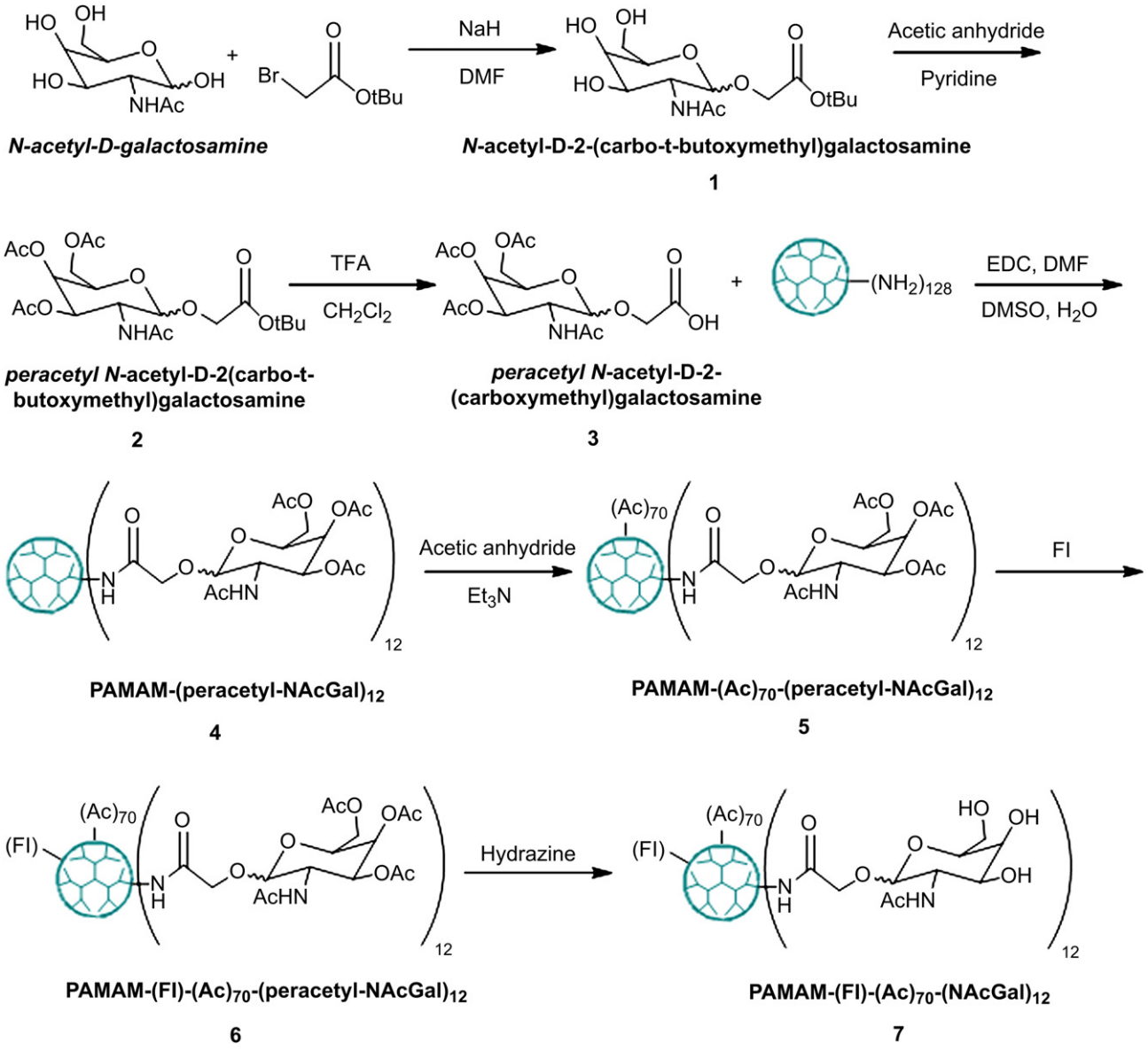

Fig. 2. Protocol for synthesis of fluorescently-labeled G5-NAcGal conjugates through a peptide linkage connecting the NAcGal ligands to the G5 carrier.

temperature for 12 h. The reaction mixture was concentrated by co-evaporation with toluene and was purified on a silica gel column using CH_2Cl_2:methanol:ethanol (10:1:0.01) as an eluent to produce 35 mg (0.086 mmol, 73% yield) of product **3** as a colorless oil. ^{1}H NMR of compound **3** in $CDCl_3$ (400 MHz Varian, Palo Alto, CA) shows δ 6.85 (br d, $J = 8.0$ Hz, 1H), 5.39 (t, $J = 8.0$ Hz, 1H), 5.20 (q,), 5.02 (d, $J = 5.0$ Hz, 1H), 4.63 (m, 1H), 4.33–4.03 (m, 5H), 2.07 (s, 3H), 2,04 (s, 3H), 2.02 (s, 3H), 1.97 (s, 3H); ESI Mass of compound **3** is 428 $[M + Na]^+$.

*2.2.4. Synthesis of 3-(PAMAM-carbamidomethyl)-2-(acetylamino)-2-deoxy-D-galactopyranoside-3,4,6-triacetate (**4**)*

1-Ethyl-3-(3-dimethylaminopropyl) carbodiimide (156.2 mg, 0.815 mmol) was added to a solution of compound **3** (33.0 mg, 0.082 mmol) dissolved in a 6 ml of dimethylformamide:dimethylsulfoxide (3:1) mixture and the reaction solution was stirred at room temperature for 1 h. G5-$(NH_2)_{128}$ dendrimer (58.5 mg, 0.00203 mmol) was added to the reaction mixture and stirred at room temperature for 72 h. The reaction was concentrated by rotary evaporation, purified by dialysis against pure water, and dried by lyophilization to produce 57 mg (0.00175 mmol, 86% yield) of compound **4** as a white solid. MALDI-TOF analysis shows that the mass for compound 4 is 32,573 g/mol.

*2.2.5. Synthesis of 3-(acetyl-PAMAM-carbamidomethyl)-2-(acetylamino)-2-deoxy-D-galactopyranoside-3,4,6-triacetate (**5**)*

Compound **4** (55 mg, 0.00169 mmol) was dissolved in 3 ml of anhydrous methanol and triethylamine (0.035 ml, 0.253 mmol) was added to the solution, followed by addition of acetic anhydride (0.0016 ml, 0.170 mmol) and stirring the reaction mixture for 20 h at room temperature. The reaction mixture was concentrated by rotary evaporation, purified by dialysis against pure water, and dried by lyophilization to produce 47 mg (0.00133 mmol, 78% yield) of product **5** as a white solid. MALDI-TOF analysis shows that the mass for compound 5 is 35,469 g/mol.

*2.2.6. Synthesis of 3-(fluorescene-acetyl-PAMAM-carbamidomethyl)-2-(acetylamino)-2-deoxy-D-galactopyranoside-3,4,6-triacetate (**6**)*

Fluorescein isothiocyanate (5 mg, 0.0133 mmol) was dissolved in 1 ml acetone and added to a solution of compound **5** (47 mg, 0.00133 mmol) dissolved in 3 ml DI water and the reaction mixture was stirred at room temperature for 24 h. The reaction mixture was concentrated by rotary evaporation, purified by dialysis against pure water, and dried by lyophilization to produce 45 mg (0.00125 mmol, 93% yield) of product **6** as an orange solid. MALDI-TOF analysis shows that the mass for compound **6** is 35,997 g/mol.

*2.2.7. Synthesis of 3-(fluorescene-acetyl-PAMAM-carbamidomethyl)-2-(acetylamino)-2-deoxy-D-galactopyranoside (**7**)*

Hydrazine monohydrate (0.4 ml, 8.24000 mmol) was added to a solution of compound **6** (45 mg, 0.00125 mmol) dissolved in 3 ml of anhydrous methanol and the reaction mixture was stirred at room temperature for 36 h. The reaction solution was concentrated by rotary evaporation, purified by dialysis against pure water, and dried by lyophilization to produce 40 mg (0.00111 mmol, 89% yield) of fluorescently-

labeled G5-NAcGal conjugates (**7**) as an orange solid. MALDI-TOF analysis shows that the mass for **7** is 35,857 g/mol.

2.3. Synthesis of fluorescently-labeled G5-NAcGal conjugates via thiourea linkages

2.3.1. Synthesis of 3-bromopropyl-2-(acetylamino)-2-deoxy-D-galactopyranoside (*8*)

Acetyl chloride (1.68 ml) was added dropwise to a solution of NAcGal (2.0 g, 9.0 mmol) in 3-bromo-L-propanol (30 ml) at 0 °C. The reaction mixture was stirred for 5.5 h at 70 °C before neutralizing the reaction mixture with Dowex-OH resin. The reaction mixture was filtered and the filtrate was purified on a silica gel column using CH_2Cl_2:methanol (3:2) as an eluent to isolate pure compound **8** (2.6 g, 7.6 mmol, 84% yield). ^{1}H NMR of compound **8** in CD_3OD (300 MHz Varian, Palo Alto, CA) shows δ 1.98 (s, 3H); 2.07–2.18 (m, 2H); 3.47–3.67 (m, 3H), 3.68–3.98 (m, 6H), 4.26 (dd, 1H, $J_1 = 3.5$ Hz, $J_2 = 11.1$ Hz); 4.83 (d, 1H, $J = 3.5$ Hz); ESI Mass for compound **8** is 364 $[M + Na]^+$.

2.3.2. Synthesis of 3-bromopropyl-2-(acetylamino)-2-deoxy-D-galactopyranoside-3,4,6-triacetate (*9*)

Excess pyridine (5 ml, 61.89 mmol) and acetic anhydride (10 ml, 105.88 mmol) were added to compound **8** (2 g, 5.84 mmol) dissolved in 20 ml anhydrous dichloromethane and the reaction mixture was stirred at room temperature for 16 h. The reaction mixture was washed with saturated copper sulfate solution followed by another wash with saturated sodium bicarbonate solution to neutralize the acetic acid byproduct. The organic layer was dried over Na_2SO_4 and concentrated by rotary evaporation before loading onto a silica gel column and fractionated using CH_2Cl_2:methanol (98:2) mixture to isolate pure compound **9** (2.36 g, 5.04 mmol, 86% yield). ^{1}H NMR of compound **9** in $CDCl_3$ (300 MHz Varian, Palo Alto, CA) shows δ 1.97 (s, 3H), 2.00 (s, 3H), 2.05 (s, 3H), 2.12–2.19 (m, 2H; s, 3H), 3.47–3.67 (m, 3H), 3.84–3.97 (m, 1H), 4.04–4.22 (m, 3H), 4.53–4.64 (m, 1H), 4.91 (d, 1H, $J = 3.5$), 5.15 (dd, 1H, $J_1 = 2.9$, $J_2 = 11.1$), 5.38 (d, 1H, $J = 3.5$), 5.59 (d, 1H, $J = 9.9$); ESI Mass of compound **9** is 490 $[M + Na]^+$.

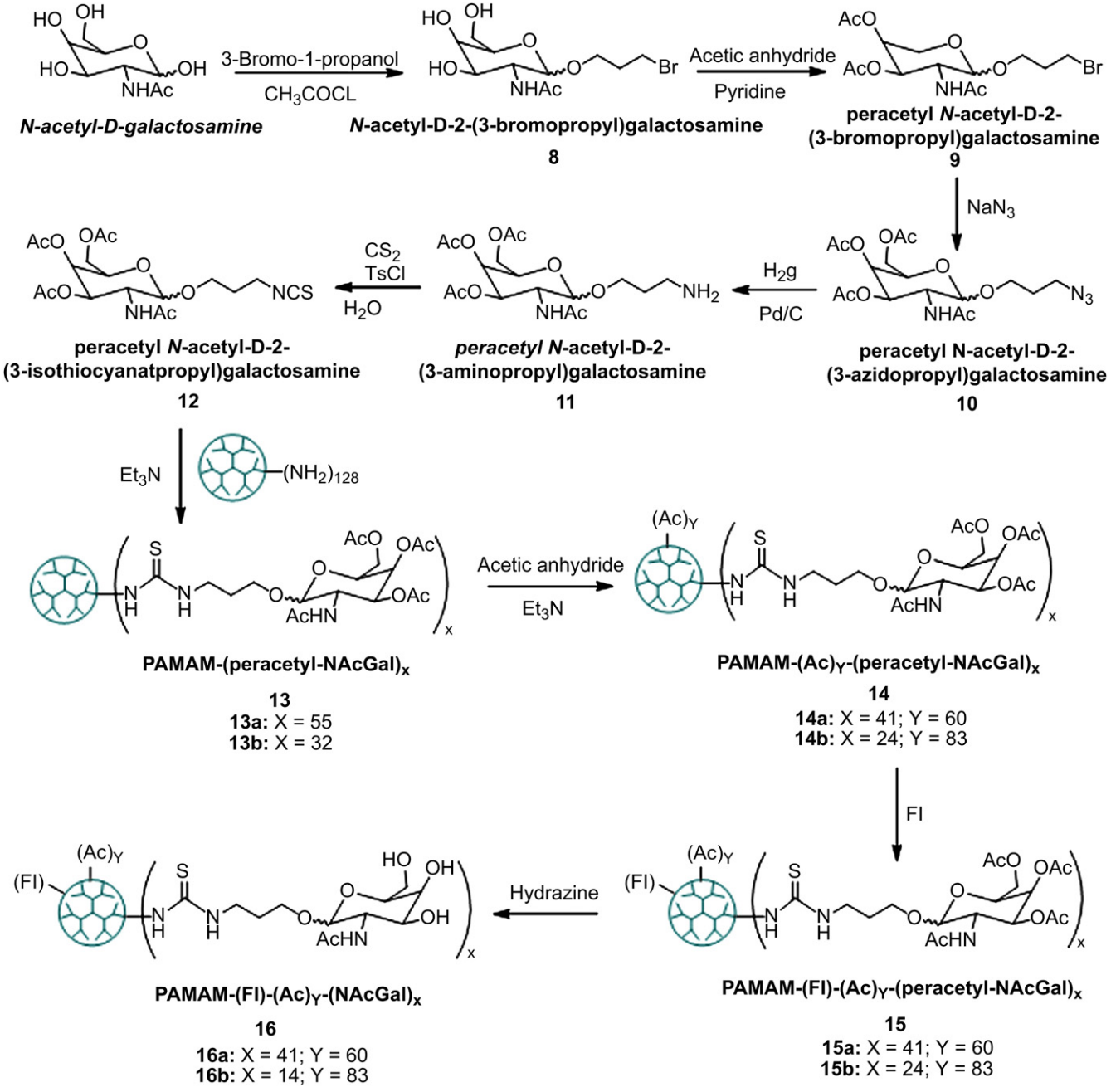

Fig. 3. Protocol for synthesis of fluorescently-labeled G5-NAcGal conjugates through a thiourea linkage connecting the NAcGal ligands to the G5 carrier.

*2.3.3. Synthesis of 3-azidopropyl-2-(acetylamino)-2-deoxy-D-galactopyranoside-3,4,6-triacetate (**10**)*

Sodium azide (0.41 g, 6.30 mmol) was added as a solid to a solution of compound **9** (1.47 g, 3.14 mmol) in 20 ml DMF and stirred for 3 h at 50 °C followed by diluting the reaction mixture with ethyl acetate, washing with ice cold water, drying over Na_2SO_4 and concentrating by rotary evaporation. The reaction mixture was purified on a silica gel column using CH_2Cl_2:acetone (9:1) mixture to produce pure compound **10** (1.33 g, 3.09 mmol, 98% yield). ^{1}H NMR of compound **10** in $CDCl_3$ (300 MHz Varian, Palo Alto, CA) shows δ 1.97 (s, 3H), 2.00 (s, 3H), 2.05 (s, 3H), 2.12–2.19 (m, 2H; s, 3H), 3.28–3.60 (m, 3H), 3.73–3.88 (m, 1H), 4.02–4.21 (m, 3H), 4.49–4.66 (m, 1H), 4.88 (d, 1H, $J = 3.5$ Hz), 5.14 (dd, 1H, $J_1 = 5.36$, $J_2 = 5.66$); ESI Mass for compound **10** is 453 $[M + Na]^+$.

*2.3.4. Synthesis of 3-isothiocyanopropyl-2-(acetylamino)-2-deoxy-D-galactopyranoside-3,4,6-triacetate (**12**)*

Compound **10** (0.8 g, 1.86 mmol) was dissolved in 30 ml ethanol and a catalytic amount of Pd/C was added to the reaction mixture and left stirring under a hydrogen blanket for 24 h. The reaction mixture was filtered and concentrated to produce the crude compound **11** (0.735 g, 1.81 mmol) that was directly used in the next reaction. Triethylamine (0.61 ml, 4.45 mmol) and carbon disulfide (0.089 ml, 1.48 mmol) were added under nitrogen to a solution of compound **11** (0.4 g, 0.99 mmol) dissolved in 20 ml tetrahydrofuran and stirred for 1 h at room temperature, followed by cooling the reaction mixture in an ice bath and adding *p*-toluenesulfonyl chloride (0.3 g, 1.58 mmol) as a solid. The reaction mixture was allowed to warm up to room temperature in 1 h followed by addition of 1 N HCl and extracting the reaction mixture using ethyl acetate. Ethyl acetate layers were dried over Na_2SO_4 and concentrated by rotary evaporation before loading on a silica gel column and isolating compound **12** (0.182 g, 0.40 mmol, 22% yield over 2 steps) using ethyl acetate:hexanes (3:2) mixture as an eluent. ^{1}H NMR of compound **12** in $CDCl_3$ (300 MHz Varian, Palo Alto, CA) shows δ 1.22–1.26 (2H, d); 1.97 (3H, s); 1.98 (3H, s); 2.02 (3H, s); 2.03 (3H, s); 3.52–3.70 (3H, m); 3.80–3.89 (1H, m); 4.04–4.16 (3H, m); 4.53–4.63 (1H, m); 4.91 (1H, d, $J = 3.5$); 5.16 (1H, dd, $J_1 = 3.5$, $J_2 = 11.1$); 5.38 (1H, d, $J = 2.9$); 5.76 (1H, d, $= J$ 9.3); ESI Mass of compound **12** is 469 $[M + Na]^+$.

*2.3.5. Synthesis of 3-((PAMAM-thioureido)propyl-2-(acetylamino))-2-deoxy-D-galactopyranoside-3,4,6-triacetate (**13a/b**)*

G5-$(NH_2)_{128}$ dendrimer (**13a**: 80 mg, 0.00277 mmol; **13b**: 60 mg, 0.00208 mmol) was dissolved in 2 ml of DI water and triethylamine (**13a**: 49.7 μL, 0.354 mmol; **13b**: 37 μL, 0.2649 mmol) was added to the reaction flask. Compound **12** (**13a**: 79 mg, 0.1774 mmol; **13b**: 29 mg, 0.0666 mmol) was dissolved in 2 ml acetone and added dropwise to the reaction mixture and stirred for 48 h at room temperature. The reaction mixture was concentrated by rotary evaporation, purified by dialysis against pure water, and lyophilized to produce 139 mg (0.0026 mmol, 94% yield) of compound **13a** and 89 mg (0.0021 mmol, 99% yield) of compound **13b**. MALDI-TOF analysis shows that the mass for **13a** is 53,468 g/mol and is 43,185 g/mol for **13b**.

*2.3.6. Synthesis of 3-((acetyl-PAMAM-thioureido)propyl-2-(acetylamino))-2-deoxy-D-galactopyranoside-3,4,6-triacetate (**14a/b**)*

Compounds **13a/b** (**13a**: 130 mg, 0.00243 mmol; **13b**: 80 mg, 0.00185 mmol) were dissolved in 3 ml of anhydrous methanol followed by addition of triethylamine (**14a**: 0.0493 ml, 0.354 mmol; **14b**: 0.0494 ml, 0.355 mmol) via a syringe and acetic anhydride (**14a**: 0.0137 ml, 0.145 mmol; **14b**: 0.0145 ml, 0.153 mmol) at room temperature. The reaction mixture was stirred at room temperature for 20 h, concentrated by rotary evaporation, purified by dialysis against pure water, and lyophilized to yield 130 mg of **14a** and 85 mg of **14b**. MALDI-TOF analysis shows that the mass for **14a** is 49,717 g/mol and is 46,671 g/mol for **14b**.

*2.3.7. Synthesis of 3-((flourescene-acetyl-PAMAM-thioureido)propyl-2-(acetylamino))-2-deoxy-D-galactopyranoside-3,4,6-triacetate (**15a/b**)*

Fluorescein isothiocyanate (Fl) (**14a**: 5.8 mg, 0.0149 mmol; **14b**: 4 mg, 0.01042 mmol) was dissolved in 0.5 ml acetone and added to an aqueous solution of compound **14a/b** (**15a**: 124 mg, 0.002494 mmol; **15b**: 75 mg, 0.001736 mmol) and kept stirring for 20 h at room temperature. The reaction mixture was concentrated by rotary evaporation and the fluorescently-labeled conjugates were purified by dialysis against pure water followed by lyopholization to yield 130 mg (0.002490 mmol, 99% yield) of compound **15a** and 77 mg (0.001635 mmol, 94% yield) of compound **15b**. MALDI-TOF analysis shows that the mass for **15a** is 52,024 g/mol and is 47,071 g/mol for **15b**.

*2.3.8. Synthesis of 3-((fluorescene-acetyl-PAMAM-thioureido)propyl-2-(acetylamino))-2-deoxy-D-galactopyranoside (**16a/b**)*

Compound **15a/b** (**15a**: 125 mg, 0.00240 mmol; **15b**: 71 mg, 0.00150 mmol) was dissolved in 3 ml of methanol and mixed with hydrazine monohydrate (**16a**: 1.16 ml, 24.02 mmol; **16b**: 0.73 ml, 15.08 mmol) was stirred for 24 h at room temperature. The reaction mixture was concentrated by rotary evaporation, purified by dialysis against pure water and lyophilized to obtain 115 mg (0.0024 mmol, 99% yield) and 57 mg (0.00139 mmol, 93% yield) of fluorescently-labeled G5-NAcGal conjugates (**16a** and **16b**), respectively. MALDI-TOF analysis shows that the mass for compound **16a** is 46,867 g/mol and is 40,934 g/mol for compound 16b.

2.4. Characterization of fluorescently-labeled G5-NAcGal conjugates

Non-acetylated G5-(Fl)-$(NH_2)_{122}$, acetylated G5-(Fl)-$(Ac)_{110}$, NAcGal-targeted G5-(Fl)-$(Ac)_{70}$-$(NAcGal)_{12}$ conjugates with a peptide linkage, and G5-(Fl)-$(Ac)_{83}$-$(NAcGal)_{14}$ and G5-(Fl)-$(Ac)_{60}$-$(NAcGal)_{41}$ conjugates with thiourea linkages were dissolved in deionized water at a concentration of 1 μM. The size and zeta potential of each conjugate were measured using a 90Plus particle size analyzer with ZetaPALS capability (Brookhaven Instruments Corporation, Holtsville, NY).

2.5. Culture of HepG2 and MCF-7 cells

HepG2 cells were cultured in T-75 flasks using MEM supplemented with 10% FBS, and 1% penicillin/streptomycin/amphotericin, sodium pyruvate, and non-essential amino acids. Similarly, MCF-7 cells were cultured using the same medium composition with the addition of 0.1% insulin solution. HepG2 cells (passages 20–25) and MCF-7 cells (passages 90–95) were incubated at 37 °C, 5% CO_2 and 95% relative humidity while changing the culture medium every 48 h. Cells were passaged at 80–90% confluency using a 0.25% trypsin-EDTA solution.

2.6. Uptake of fluorescently-labeled dendrimers into HepG2 and MCF-7 cells

HepG2 and MCF-7 cells were seeded in 24-well plates at seeding density of 5×10^5 cells/well and allowed to adhere overnight. The culture medium was aspirated and the cells were incubated for 2 or 24 h at regular culture conditions with different concentrations (5–100 nM) of non-acetylated G5-(Fl)-$(NH_2)_{122}$, acetylated G5-(Fl)-$(Ac)_{110}$, NAcGal-targeted G5-(Fl)-$(Ac)_{70}$-$(NAcGal)_{12}$ conjugates with a peptide linkage, or G5-(Fl)-$(Ac)_{83}$-$(NAcGal)_{14}$ and G5-(Fl)-$(Ac)_{60}$-$(NAcGal)_{41}$ conjugates with thiourea linkages dissolved in OPTI-MEM solution. After the selected incubation period HepG2 and MCF-7 cells were washed with cold PBS, trypsinized, and centrifuged at 1000 rpm for 5 min to pellet the cells before suspending them in 1 ml of fresh PBS and analyzing them using a Beckman Coulter FACsCalibur flow cytometer with a 488 nm excitation laser. Gating during flow analysis was based on normalized fluorescence of untreated cells to evaluate cellular internalization of each treatment as a function of conjugate's chemical composition, concentration, and incubation time. Uptake of each conjugate was evaluated in three independent experiments using four replicates for each experimental condition.

Uptake of non-acetylated G5-(Fl)-$(NH_2)_{122}$, acetylated G5-(Fl)-$(Ac)_{110}$, and NAcGal-targeted G5-(Fl)-$(Ac)_{83}$-$(NAcGal)_{14}$ conjugates into HepG2 cells (1×10^5 cells/well) upon incubation with 200 nM solution of each conjugate for 4 h was visualized using a Nikon Eclipse TE2000-U inverted microscope equipped with a photometrics EMCCD camera and an EXFO fluorescent lamp ($\lambda_{ex} = 488$ nm, $\lambda_{em} = 512$ nm). Uptake of NAcGal-targeted G5-(Fl)-$(Ac)_{83}$-$(NAcGal)_{14}$ conjugates into HepG2 cells was evaluated as a function of conjugate's concentration (5–100 nM) upon co-incubation with 100 mM of free NAcGal ligands using flow cytometry to determine the role of the ASGPR in the internalization of NAcGal-targeted conjugates into hepatic cancer cells.

2.7. Cytotoxicity of fluorescently-labeled G5-NAcGal conjugates

Toxicity of non-acetylated G5-(Fl)-$(NH_2)_{122}$, acetylated G5-(Fl)-$(Ac)_{110}$, NAcGal-targeted G5-(Fl)-$(Ac)_{70}$-$(NAcGal)_{12}$ conjugates with a peptide linkage, and G5-(Fl)-$(Ac)_{83}$-$(NAcGal)_{14}$ and G5-(Fl)-$(Ac)_{60}$-$(NAcGal)_{41}$ conjugates with thiourea linkages was evaluated using the lactate dehydrogenase (LDH) leakage assay (Roche Diagnostics Corporation, Indianapolis, IN) at a concentration of a 100 nM, which is the highest concentration used in the uptake studies. Briefly, HepG2 cells were seeded in 24-well plates at a seeding density of 5×10^5 cells/well and allowed to adhere overnight before replacing the culture medium with OPTI-MEM solution containing different conjugates and incubating for 2 and 24 h under normal culture conditions. The amount of LDH enzyme present in the culture medium after incubation with each conjugate was quantified by mixing 100 μl of the culture medium with 100 μl of the enzyme substrate included in the assay kit following the manufacturer's guidelines, and measuring the absorbance of this mixture at 490 nm using a Multiskan microplate reader (Thermo Fisher Scientific Inc., Waltham, MA). Contribution of the fluorescent and sugar molecules to the absorbance of each conjugate was eliminated by subtracting the absorbance of a 100 nM solution of each conjugate at 490 nm. LDH leakage observed upon incubation of HepG2 cells with OPTI-MEM culture medium and 2% v/v Triton X-100 solution were used as negative and positive controls, respectively. The amount of LDH enzyme present in the culture medium upon incubation of each conjugate with HepG2 cells was normalized to the amount of LDH observed upon incubation of HepG2 cells with 2% v/v Triton X-100 solution. G5-NAcGal conjugates that result in statistically higher LDH leakage compared to the negative control (blank OPTI-MEM culture medium) were considered cytotoxic.

3. Results and discussion

3.1. Synthesis of fluorescently-labeled G5-NAcGal conjugates

One successful strategy to target drug carriers to hepatic cancer cells is to covalently conjugate NAcGal sugar molecules to the

polymer backbone [20,21] or to the surface of the polymeric particle[22,23]. Earlier reports showed that conjugation of 10 mol% galactose molecules to *N*-(2-hydroxypropyl)methacrylamide (HPMA) polymers increased their uptake into HepG2 cells compared to non-targeted carriers [20]. Consequently, we reacted NAcGal molecules functionalized with a carboxylic acid group with G5-$(NH_2)_{128}$ dendrimers at a COOH-to-NH_2 ratio of 13:128 following the synthesis scheme shown in Fig. 2. Coupling of NAcGal-COOH ligands to G5-$(NH_2)_{128}$ dendrimers via peptide linkage yielded G5-$(NAcGal)_{12}$ conjugates (Fig. 2, Compound **4**) with 9.4 mol% of NAcGal molecules as determined by MALDI-TOF analysis. To evaluate the effect of linkage chemistry on the internalization of G5-NAcGal conjugates, NAcGal molecules were functionalized with an isothiocyanate group to allow their coupling to G5-$(NH_2)_{128}$ dendrimers via a thiourea linkage following the synthesis scheme shown in Fig. 3. We varied the amount of NAcGal molecules used in the coupling reaction to achieve 10 mol% and 40 mol% capping of the NH_2 surface groups, which yielded G5-(Fl)-$(Ac)_{83}$-$(NAcGal)_{14}$ and G5-(Fl)-$(Ac)_{60}$-$(NAcGal)_{41}$ conjugates (Fig. 3, Compounds **16a** and **16b)** containing 10.9 mol% and 32.0 mol% NAcGal ligands, respectively. G5-NAcGal conjugates were reacted with acetic anhydride to neutralize a major fraction of the primary amine surface groups and minimize the contribution of non-specific adsorptive-mediated endocytosis to the internalization of these conjugates yielding acetylated G5-NAcGal conjugates (Fig. 2, Compound **5**; Fig. 3, Compounds **14a** and **14b)**. To quantify the amount of each conjugate internalized by HepG2 and MCF-7 cells and visualize their intracellular distribution, we fluorescently labeled all G5-NAcGal conjugates by reacting with fluorescein isothiocyanate (Fl) following published protocols [24,25]. Approximately 4 ± 2 fluorescein isothiocyanate molecules were attached per G5-NAcGal conjugate, which matches the reported values and provide sufficient fluorescence signals for analysis of conjugate's uptake into HepG2 and MCF-7 cells. The acetyl groups used to cap the hydroxyl groups of the coupled NAcGal molecules were removed after the fluorescence labeling of all G5-NAcGal conjugates using hydrazine to yield the final fluorescently-labeled G5-NAcGal conjugates (Fig. 2, Compound **7**; Fig. 3, Compounds **16a** and **16b)** used in all the uptake studies.

3.2. Size and surface charge of fluorescently-labeled G5-NAcGal conjugates

Earlier research showed that internalization of PAMAM-NH_2 dendrimers is mediated by electrostatic interaction between the cationic primary amine surface groups and the negatively charged proteoglycans displayed on the surface of mammalian cells, which triggers macropinocytosis [26] and clathrin-mediated endocytosis [26–28] of these particles into different cell lines. Internalization of PAMAM-NH_2 dendrimers into mammalian cells proved to increase with the increase in their size and positive charge density [26–31]. To achieve selective drug delivery into hepatic cancer cells using G5-NAcGal conjugates as carriers, it is critical to neutralize the free primary amine surface groups thus limiting the internalization of these conjugates to receptor-mediated endocytosis through the interaction of the NAcGal ligands and the ASGPR expressed on the surface of hepatic cancer cells while minimizing the contribution of non-specific adsorptive-mediated endocytosis to conjugate's uptake. Further, G5-NAcGal conjugates should be 5–8 nm in size to reduce their diffusion across the endothelial lining of normal blood vessels, increase their extravasation across tumor vasculature, and diminish their recognition and entrapment by the reticular endothelial system [13,32,33].

Our results show that the average size of G5-$(Fl)_6$-$(NH_2)_{122}$ is 4.75 ± 0.73 nm **(**Fig. 4, Panel A**)**, which closely matches the reported size (5 nm) of non-labeled G5-$(NH_2)_{128}$ dendrimers [34]. Results also show that G5-$(Fl)_6$-$(NH_2)_{122}$ dendrimers carry a net positive charge of 7.14 ± 1.02 mV (Fig. 4, Panel B**)** due to the ionization of the free primary amine surface groups, which have a reported pKa value of 10.8 [35–37]. Acetylation of 110 (86%) of the primary amine surface groups slightly increased the average size of G5-$(Fl)_6$-$(Ac)_{110}$ dendrimers to 5.00 ± 1.44 nm and completely abolished the positive surface charge of this carrier as shown by the drop in zeta potential to −0.17 ± 0.64 mV (Fig. 4). Acetylation of 70 (55%) of the primary amine surface groups, coupling of 12 NAcGal molecules (9.4%), and fluorescence-labeling of G5-$(NH_2)_{128}$ dendrimers yields G5-$(Fl)_6$-$(Ac)_{70}$-$(NAcGal)_{12}$ conjugates with an average size of 6.13 ± 1.00 nm and average zeta potential of 0.25 ± 2.08 mV. Similarly, acetylation of 83 (65%) of the primary amine surface groups, coupling of 14 NAcGal molecules (11%), and fluorescence-labeling of G5-$(NH_2)_{128}$ dendrimers yields G5-$(Fl)_6$-$(Ac)_{83}$-$(NAcGal)_{14}$ conjugates with an average size of 6.02 ± 0.83 nm and an average zeta potential of 0.62 ± 1.32 mV. Increasing the number of NAcGal molecules conjugated to G5-$(NH_2)_{128}$ dendrimers to 41 (32%) along with acetylation of 60 (47%) primary amine surface groups yields G5-$(Fl)_6$-$(Ac)_{60}$-$(NAcGal)_{41}$ conjugates with an average size of 6.74 ± 2.05 nm and an average zeta potential of 0.66 ± 0.33 mV.

Results show that covalent coupling of NAcGal molecules to G5-$(NH_2)_{128}$ dendrimers with variable degrees of acetylation caused a gradual increase in conjugate size with the increase in the number of attached NAcGal ligands (Fig. 4, Panel A) particularly for conjugates incorporating thiourea linkages, which have a longer spacer between the sugar molecule and the dendrimer surface compared to the spacer used in peptide coupling (Figs. 2 and 3). However, the average size of all the synthesized G5-NAcGal conjugates remained within the desirable size range (5–8 nm). Coupling of NAcGal and Fl molecules to G5 dendrimers along with variable degrees of acetylation resulted in capping 69%–84% of the primary amine surface groups in G5-NAcGal conjugates, which successfully reduced the cationic nature of these conjugates shown by the statistically significant drop in zeta potential of G5-$(Fl)_6$-$(Ac)_{70}$-$(NAcGal)_{12}$, G5-$(Fl)_6$-$(Ac)_{83}$-$(NAcGal)_{14}$, and G5-$(Fl)_6$-$(Ac)_{60}$-$(NAcGal)_{41}$ conjugates compared to G5-$(Fl)_6$-$(NH_2)_{122}$ dendrimers (Fig. 4, Panel B). Reduction in positive surface charge of G5-NAcGal conjugates will minimize their *in vivo* opsonization and non-specific uptake into non-targeted cells. It is important to note that fluorescence labeling, acetylation, and coupling of NAcGal molecules to G5-$(NH_2)_{128}$ dendrimers did not affect its intrinsic aqueous solubility. All the fluorescently-labeled G5-NAcGal conjugates were freely soluble in water, buffers, and cell culture medium at all the concentrations used in the reported uptake studies.

3.3. Uptake of cationic G5-(Fl)-(NH_2) dendrimers into HepG2 and MCF-7 cells

Results show that uptake of cationic G5-(Fl)-$(NH_2)_{122}$ dendrimers by HepG2 and MCF-7 cells increases with the increase in carrier concentration and incubation time (Fig. 5). Specifically, the fraction of HepG2 and MCF-7 cells that internalized G5-(Fl)-$(NH_2)_{122}$ particles after 2 h of incubation increased linearly with the increase in carrier concentration reaching 90–100% of the cell population at 50 nM particle concentration (Fig. 5, Panel A). Incubation with a higher concentration (100 nM) of G5-(Fl)-$(NH_2)_{122}$ particles produced a statistically insignificant increase in the fraction of HepG2 and MCF-7 cells internalizing these particles. Increasing the incubation time to 24 h produced a corresponding increase in the fraction of HepG2 and MCF-7 cells taking up G5-(Fl)-$(NH_2)_{122}$ particles at 5, 10, and 25 nM concentrations compared to shorter incubation time (Fig. 5, Panel B**)**. Incubation of HepG2 and MCF-7

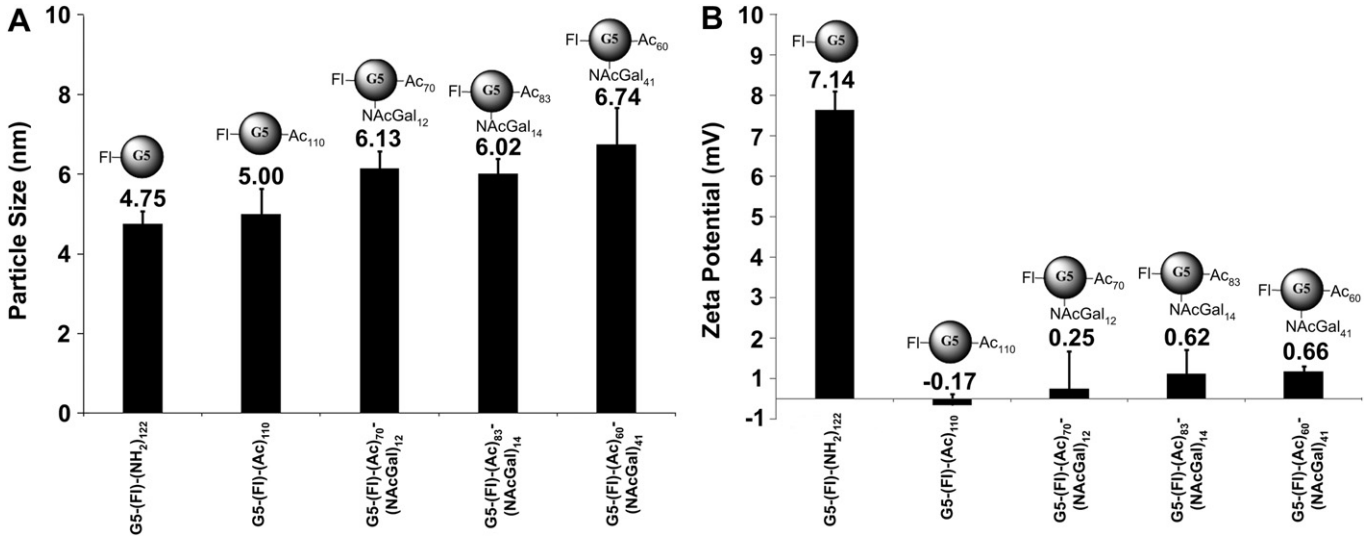

Fig. 4. Particle size (A) and zeta potential (B) of non-acetylated G5-(Fl)-$(NH_2)_{122}$, acetylated G5-(Fl)-$(Ac)_{110}$, and NAcGal-targeted G5-(Fl)-$(Ac)_{70}$-$(NAcGal)_{12}$, G5-(Fl)-$(Ac)_{83}$-$(NAcGal)_{14}$, G5-(Fl)-$(Ac)_{83}$-$(NAcGal)_{41}$ conjugates.

cells with 50 and 100 nM solutions of G5-(Fl)-$(NH_2)_{122}$ particles for 24 h led to their uptake by almost 100% of the cell population.

HepG2 and MCF-7 cells exhibited similar uptake of G5-(Fl)-$(NH_2)_{122}$ dendrimers at both incubation time points except at the lowest concentration (5 nM) where the fraction of HepG2 cells that internalized these cationic particles was twice as much as the fraction of MCF-7 cells that internalized the same particle under similar conditions, which can be attributed to the higher endocytic capacity of hepatic cells toward synthetic particles [38]. This difference in uptake between HepG2 and MCF-7 cells was not observed at higher concentrations of G5-(Fl)-$(NH_2)_{122}$ dendrimers because the number of particles present in solution is no longer a limiting factor. The inability of G5-(Fl)-$(NH_2)_{122}$ dendrimers to discriminate between HepG2 and MCF-7 cells is a result of the protonation of 99% of the NH_2 surface groups (pKa of 10.8) at physiologic pH, which confers a high positive charge density on the particle surface leading to electrostatic interaction with the negatively charged proteoglycans displayed on the surface of HepG2 and MCF-7 cells that triggers adsorptive-mediated endocytosis of these particles. These results are in agreement with earlier reports showing non-selective internalization of cationic dendrimers by Caco-2 [28,30], A592 lung epithelium [39], and B16f10 melanoma [40] cells via adsorptive-mediated endocytosis. We conjugated NAcGal molecules and acetylated the free NH_2 surface groups to switch the internalization mechanism of these carriers from non-specific adsorptive-mediated endocytosis to selective uptake by receptor-mediated endocytosis into hepatic cells.

3.4. Uptake of G5-NAcGal conjugates into HepG2 cells

We compared the uptake of acetylated, non-targeted, G5-(Fl)-$(Ac)_{110}$ to NAcGal-targeted G5-(Fl)-$(Ac)_{70}$-$(NAcGal)_{12}$ conjugates prepared through peptide coupling, and G5-(Fl)-$(Ac)_{83}$-$(NAcGal)_{14}$ and G5-(Fl)-$(Ac)_{60}$-$(NAcGal)_{41}$ conjugates incorporating a thiourea linkage (Fig. 6). Results show that acetylated, non-targeted, G5-(Fl)-$(Ac)_{110}$ conjugates were internalized by only 10% of HepG2 cells after incubation with a 100 nM solution of the particles for 2 h (Fig. 6, Panel A), which is a significantly lower uptake compared to cationic G5-(Fl)-$(NH_2)_{122}$ dendrimers (Fig. 5, Panel A). Specifically, uptake of the neutral G5-(Fl)-$(Ac)_{110}$ dendrimers into HepG2 cells was reduced by 50-fold compared to cationic G5-(Fl)-$(NH_2)_{122}$ particles as a result of 7.5-fold reduction in the number of free NH_2

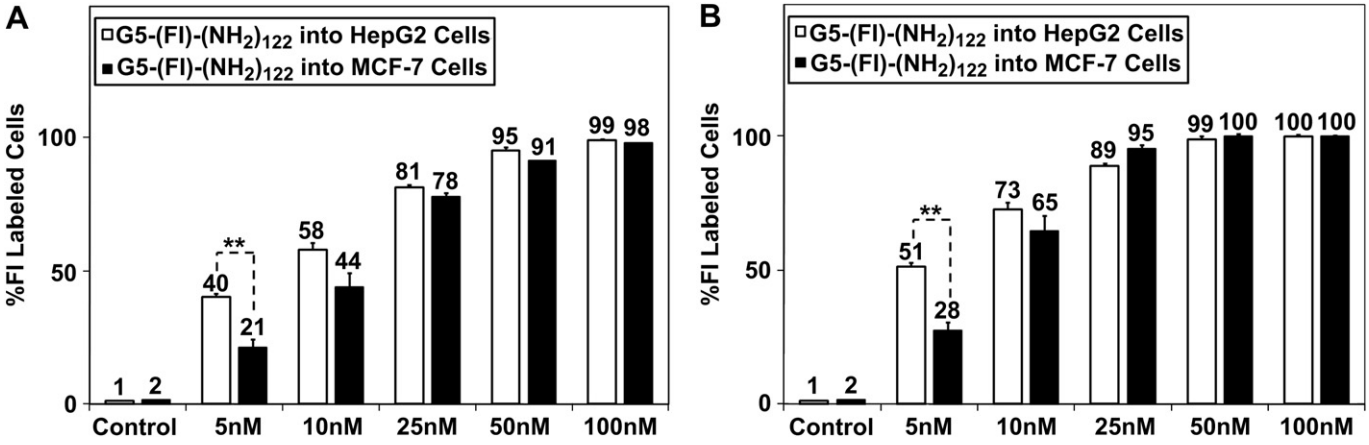

Fig. 5. Uptake of cationic G5-(Fl)-$(NH_2)_{122}$ conjugates into HepG2 and MCF-7 upon incubation for 2 (A) and 24 h (B). Results are the average of four samples + standard error of the mean. Statistical difference between groups is denoted by **, which indicates that $p \leq 0.01$.

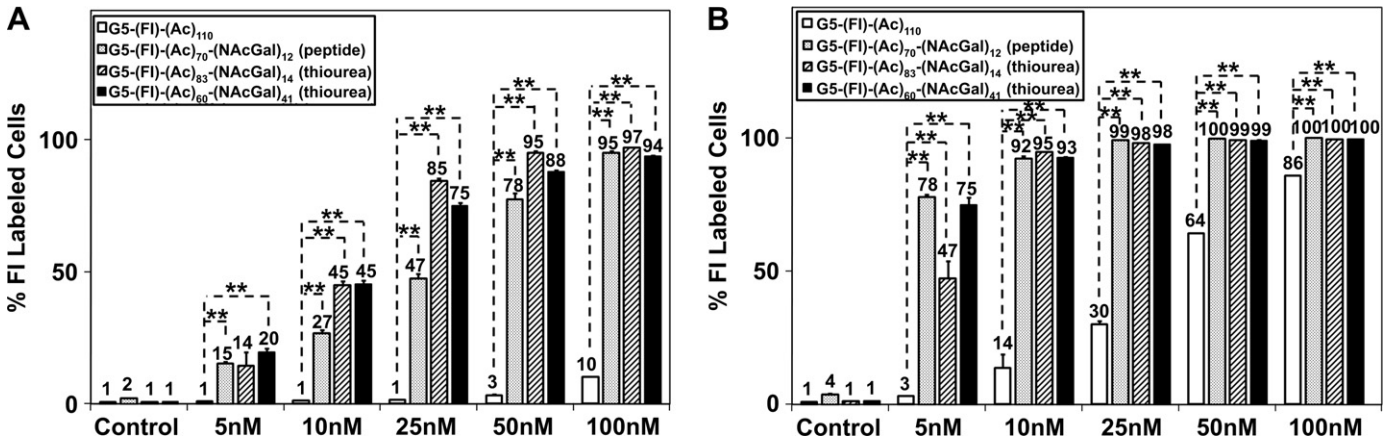

Fig. 6. Uptake of acetylated G5-(Fl)-$(Ac)_{110}$ dendrimers, G5-(Fl)-$(Ac)_{70}$-$(NAcGal)_{12}$ conjugates incorporating peptide linkages, and G5-(Fl)-$(Ac)_{83}$-$(NAcGal)_{14}$ and G5-(Fl)-$(Ac)_{83}$-$(NAcGal)_{41}$ conjugates incorporating thiourea linkages into HepG2 cancer cells upon incubation for 2 (A) and 24 h (B). Results are the average of four samples + standard error of the mean. Statistical difference between groups is denoted by **, which indicates that $p \leq 0.01$.

surface groups, which clearly confirms the role of positive surface charge in the internalization of G5-(Fl)-$(NH_2)_{122}$ conjugates into hepatic cancer cells. Incubation of HepG2 cells with 100 nM solution of neutral G5-(Fl)-$(Ac)_{110}$ dendrimers for 24 h led to internalization of these particles by 86% of HepG2 cells, which is a result of the higher particle concentration and longer incubation time leading to fluid-phase endocytosis of these particles as shown in earlier reports [41].

Despite the similarity in size and surface charge (Fig. 4), all G5-NAcGal conjugates exhibited higher uptake into HepG2 cells compared to non-targeted G5-(Fl)-$(Ac)_{110}$ dendrimers at all concentrations and incubation times (Fig. 6). For example, the fraction of HepG2 taking up G5-(Fl)-$(Ac)_{70}$-$(NAcGal)_{12}$ conjugates increased from 15% to 95% with the increase in conjugate concentration from 5 nM to 100 nM compared to non-targeted G5-(Fl)-$(Ac)_{110}$ dendrimers, which was internalized by 10% of HepG2 cells at the highest tested concentration, 100 nM (Fig. 6A). After incubation for 24 h, G5-(Fl)-$(Ac)_{70}$-$(NAcGal)_{12}$ conjugates showed a much higher uptake into HepG2 cells reaching 78% of the cell population at a 5 nM concentration, which is 26-folds higher than the non-targeted G5-(Fl)-$(Ac)_{110}$ dendrimers at the same concentration (Fig. 6B). Increasing the concentration of G5-(Fl)-$(Ac)_{70}$-$(NAcGal)_{12}$ conjugates to 10 nM saturates the internalization process with more than 92% of HepG2 cells taking up this NAcGal-targeted conjugate compared to only 14% of the non-targeted G5-(Fl)-$(Ac)_{110}$ dendrimers. These results clearly show the significantly enhanced uptake of NAcGal-functionalized G5 dendrimers into hepatic cancer cells over non-targeted G5 dendrimers.

We compared the uptake of G5-(Fl)-$(Ac)_{70}$-$(NAcGal)_{12}$ conjugates synthesized via peptide coupling to that of G5-(Fl)-$(Ac)_{83}$-$(NAcGal)_{14}$ and G5-(Fl)-$(Ac)_{60}$-$(NAcGal)_{41}$ conjugates incorporating a thiourea linkage as a function of conjugate's concentration and incubation time to evaluate the effect of linkage chemistry on the internalization of NAcGal-targeted conjugates into HepG2 cells. After 2 h of incubation with HepG2 cells, uptake of peptide-linked G5-(Fl)-$(Ac)_{70}$-$(NAcGal)_{12}$ conjugates was similar to conjugates incorporating a thiourea linkage at 5 nM, 50 nM and 100 nM concentrations, but was lower by 40% at 10 nM and 25 nM concentrations (Fig. 6A). After 24 h of incubation with HepG2 cells, uptake of peptide-linked G5-(Fl)-$(Ac)_{70}$-$(NAcGal)_{12}$ conjugates was equivalent to the G5-NAcGal conjugates incorporating a thiourea linkage at almost all the tested concentrations. It is clear that there is a difference in uptake between peptide- and thiourea-linked G5-NAcGal conjugates at short incubation times likely due to the longer spacer arms (5 atoms) connecting the NAcGal ligands to the G5 carrier in the thiourea linkage compared to the peptide linkage (3 atoms), which will results in a better display and recognition of the anchored NAcGal ligands.

NAcGal-targeted conjugates containing a thiourea linkage showed much higher internalization into HepG2 cells compared to non-targeted G5-(Fl)-$(Ac)_{110}$ conjugates at 10–100 nM and 5–100 nM concentration for G5-(Fl)-$(Ac)_{83}$-$(NAcGal)_{14}$ and G5-(Fl)-$(Ac)_{60}$-$(NAcGal)_{41}$ conjugates, respectively (Fig. 6). G5-(Fl)-$(Ac)_{83}$-$(NAcGal)_{14}$ and G5-(Fl)-$(Ac)_{60}$-$(NAcGal)_{41}$ conjugates showed similar uptake into HepG2 cells at all concentrations and incubation times despite the difference in their NAcGal content, which suggests that conjugation of 10 mol% of NAcGal molecules per G5 dendrimer is sufficient to achieve maximal internalization into hepatic cancer cells. In addition, results show that G5-NAcGal conjugates are efficiently internalized into HepG2 cells compared to linear polymers like HPMA-NAcGal conjugates incorporating 14.8 mol%, which are internalized by only 25% of HepG2 cells after 2 h of incubation at a much higher concentration of 667 nM [20]. For example, incubation of a 50 nM solution of G5-NAcGal conjugates with HepG2 cells for 2 h results in conjugate internalization by 95% of HepG2 cells, which is 4-fold higher than the reported uptake of linear HPMA-NAcGal conjugates incubated at a 13-fold higher concentration indicating the higher affinity and selectivity of G5-NAcGal conjugates toward hepatic cancer cells compared to linear carriers.

Further, we visualized the uptake and intracellular distribution of cationic G5-(Fl)-$(NH_2)_{122}$, acetylated G5-(Fl)-$(Ac)_{110}$, and NAcGal-targeted G5-(Fl)-$(Ac)_{83}$-$(NAcGal)_{14}$ conjugates into HepG2 cells using fluorescence microscopy (Fig. 7). After a 4 h incubation of HepG2 cells with a 200 nM solution of each conjugate, fluorescence images show that cationic G5-(Fl)-$(NH_2)_{122}$ conjugates are readily internalized by HepG2 cells while neutral G5-(Fl)-$(Ac)_{110}$ conjugates are poorly taken up into the cells, which provides a clear visual evidence on the effect of positive charge on triggering non-specific adsorptive-mediated endocytosis of cationic dendrimers into hepatic cancer cells. HepG2 cells incubated with G5-(Fl)-$(Ac)_{83}$-$(NAcGal)_{14}$ conjugates showed high fluorescence intensity in membrane-bound vesicles such as the endosomes and lysosomes, along with diffuse distribution throughout the cytoplasm (Fig. 7). These images provide additional evidence that NAcGal ligands enhance the cellular uptake of G5-NAcGal conjugates through receptor-mediated endocytosis. The combination of punctuate and diffuse fluorescence in HepG2 cells incubated with G5-(Fl)-$(Ac)_{83}$-$(NAcGal)_{14}$ conjugates show the ability of the G5 carrier to escape the endosomal membrane and enter the cytoplasm through the proton sponge mechanism [7,42,43]. The ability of G5-NAcGal

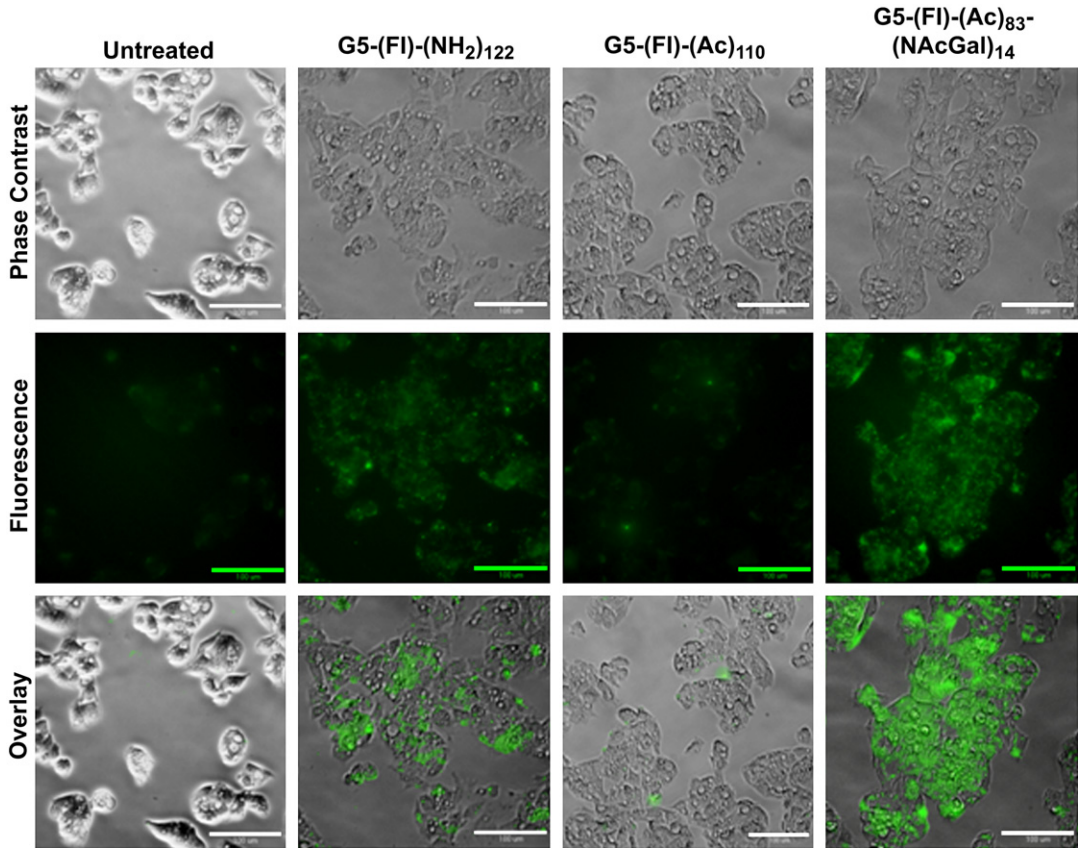

Fig. 7. Phase contrast and fluorescence images showing the internalization and intracellular distribution of cationic G5-(Fl)-$(NH_2)_{122}$, acetylated G5-(Fl)-$(Ac)_{110}$, and G5-(Fl)-$(Ac)_{83}$-$(NAcGal)_{14}$ conjugates into HepG2 cells visualized at a 20× magnification (scale bar = 100 μm) using a Nikon Eclipse TE2000-U inverted microscope with a Photometrics EMCCD camera and EXFO fluorescent lamp (λ_{ex} = 488 nm, λ_{em} = 512 nm).

conjugates to escape the endosomal/lysosomal trafficking pathway and enter the cytoplasm indicates their ability to function as vehicles for efficient delivery of anticancer drugs into the cytoplasm of hepatic cancer cells.

3.5. Role of ASGPR in HepG2 uptake of G5-NAcGal conjugates

We carried out a competitive uptake study to confirm the contribution and specificity of the ASGPR to the internalization of G5-NAcGal conjugates into HepG2 cells. In this study, we compared the uptake of G5-(Fl)-$(Ac)_{83}$-$(NAcGal)_{14}$ conjugates into HepG2 cells in the presence of excess (100 mM) free NAcGal molecules in the culture medium to the conjugates uptake in the absence of free sugar molecules as a function of G5-NAcGal conjugate concentration and incubation time (Fig. 8). In the absence of free NAcGal molecules, uptake of G5-(Fl)-$(Ac)_{83}$-$(NAcGal)_{14}$ conjugate into HepG2 cells increase with the increase in conjugate concentration, reaching maximum uptake upon incubation with 100 nM and 10 nM conjugate solutions for 2 and 24 h, respectively (Fig. 8). However, co-incubation of free NAcGal with G5-(Fl)-$(Ac)_{83}$-$(NAcGal)_{14}$ conjugate led to

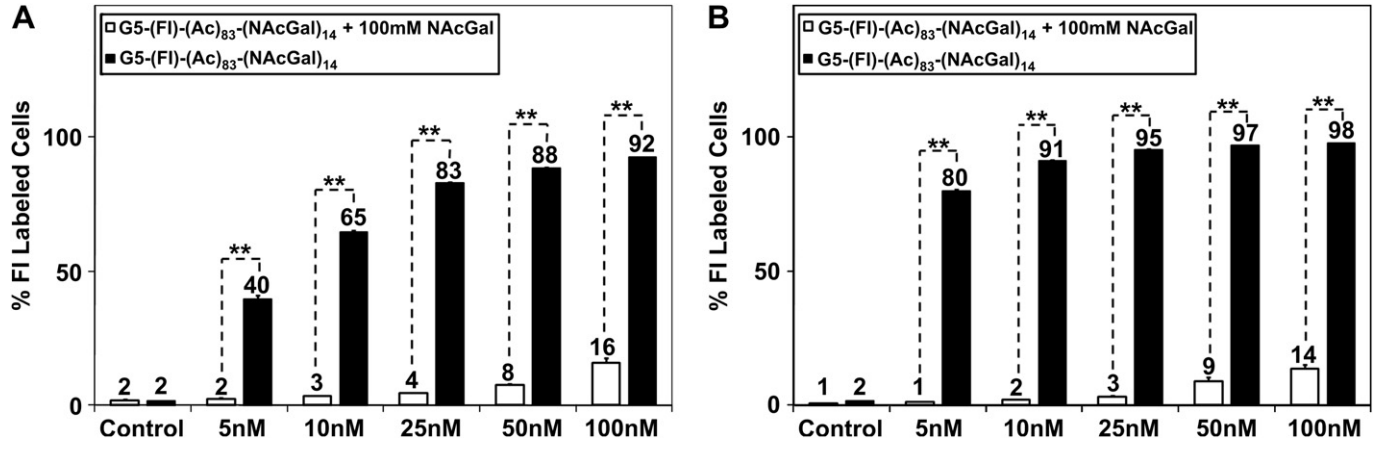

Fig. 8. Uptake of G5-(Fl)-$(Ac)_{83}$-$(NAcGal)_{14}$ conjugates into HepG2 cells upon co-incubation with 100 mM of free NAcGal molecules for 2 (A) and 24 h (B) of incubation. Results are the average of four samples + standard error of the mean. Statistical difference between groups is denoted by **, which indicates that $p \leq 0.01$.

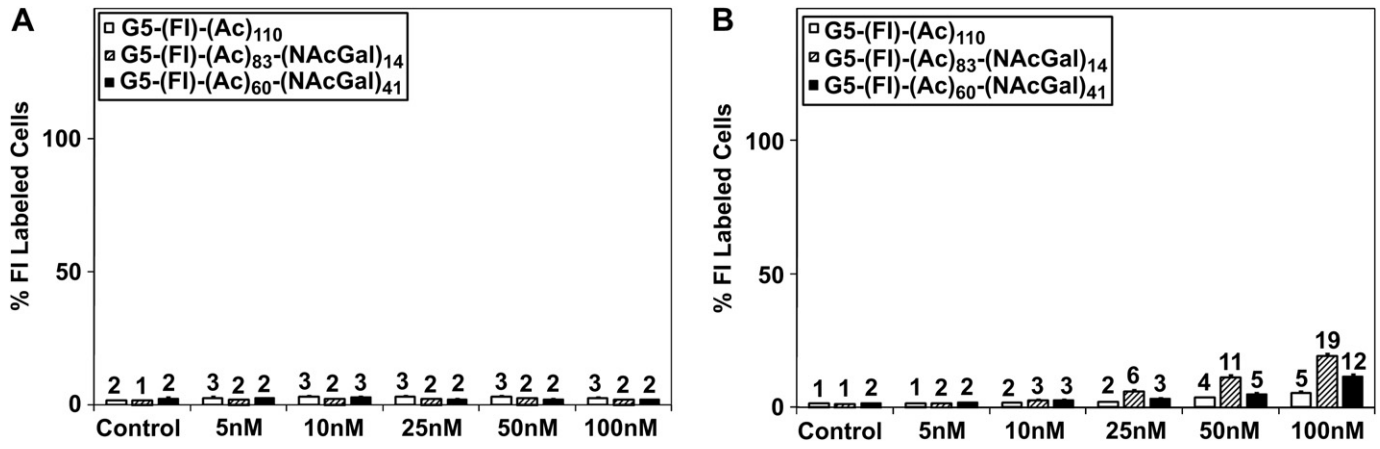

Fig. 9. Uptake of acetylated G5-(Fl)-$(Ac)_{110}$, G5-(Fl)-$(Ac)_{83}$-$(NAcGal)_{14}$, and G5-(Fl)-$(Ac)_{83}$-$(NAcGal)_{41}$ conjugates into MCF-7 breast cancer cells upon incubation for 2 (A) and 24 h (B). Results are the average of four samples + standard error of the mean.

a statistically significant ($p \leq 0.01$) reduction in conjugate's uptake into HepG2 cells with only 14% of the cell population taking up the conjugate after 24 h of incubation (Fig. 8, Panel B). The observed reduction in the uptake of G5-(Fl)-$(Ac)_{83}$-$(NAcGal)_{14}$ conjugate into HepG2 cells upon co-incubation with free NAcGal molecules is explained by previous studies showing that the binding and internalization of the ASGPR follow Michaelis–Menten kinetics [44]. Presence of excess free NAcGal that can effectively compete for and bind to the ASGPR will saturate the receptors and reduce their availability to bind and internalize the G5-(Fl)-$(Ac)_{83}$-$(NAcGal)_{14}$ conjugates present in solution, which will reduce their net uptake into HepG2 cells. This clearly demonstrates that uptake of G5-NAcGal conjugates into hepatic cancer cells occurs through the ASGPR via receptor-mediated endocytosis. Our results are supported by a previous study where uptake of NAcGal-targeted HPMA conjugates into HepG2 cells was inhibited by co-incubation with excess lactose molecules [20].

Selectivity of G5-NAcGal for hepatic cancer cells was investigated by incubating non-targeted G5-(Fl)-$(Ac)_{110}$, G5-(Fl)-$(Ac)_{83}$-$(NAcGal)_{14}$, and G5-(Fl)-$(Ac)_{60}$-$(NAcGal)_{41}$ conjugates with MCF-7 breast cancer cells, which do not express the ASGPR essential for internalization of NAcGal-targeted conjugates. Results show that MCF-7 cells exhibit negligible uptake ($\leq$3%) of both NAcGal-targeted and non-targeted G5 conjugates upon incubation for 2 h at all the tested concentrations (Fig. 9, Panel A). Incubation of MCF-7 cells with NAcGal-targeted and non-targeted G5 conjugates for 24 h also showed limited conjugate uptake with only 19% of the MCF-7 cells internalizing G5-(Fl)-$(Ac)_{83}$-$(NAcGal)_{14}$ conjugates, which can be attributed to non-specific fluid-phase endocytosis (Fig. 9, Panel B). The limited uptake of G5-NAcGal conjugates into MCF-7 cells compared to HepG2 cells confirms the selectivity of these targeted polymers toward hepatic cancer cells and suggests their potential as drug carriers targeted to hepatic cancer cells.

3.6. Cytotoxicity of fluorescently-labeled G5-NAcGal conjugates

Biocompatibility and lack of cellular toxicity are essential requirements for successful use of G5-NAcGal conjugates as carriers for targeted drug delivery into hepatic cancer cells. Consequently, we examined the toxicity of cationic G5-(Fl)-$(NH_2)_{122}$, acetylated G5-(Fl)-$(Ac)_{110}$, and NAcGal-targeted G5-(Fl)-$(Ac)_{70}$-$(NAcGal)_{12}$, G5-(Fl)-$(Ac)_{83}$-$(NAcGal)_{14}$, and G5-(Fl)-$(Ac)_{60}$-$(NAcGal)_{41}$ conjugates

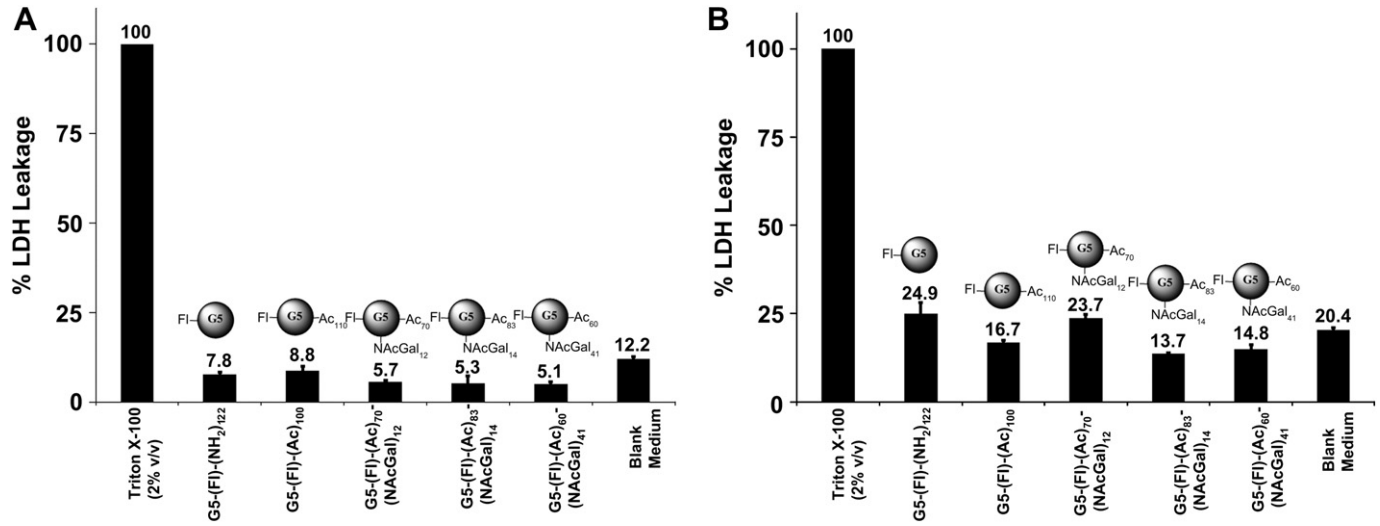

Fig. 10. Percentage of LDH leakage observed after incubation of 100 nM solutions of cationic G5-(Fl)-$(NH_2)_{122}$, acetylated G5-(Fl)-$(Ac)_{110}$, G5-(Fl)-$(Ac)_{70}$-$(NAcGal)_{12}$, G5-(Fl)-$(Ac)_{83}$-$(NAcGal)_{14}$, and G5-(Fl)-$(Ac)_{83}$-$(NAcGal)_{41}$ conjugates with HepG2 cells for 2 (A) and 24 h (B). LDH leakage for each treatment is normalized to that observed upon incubation of HepG2 cells with 2% (v/v) Triton X-100 solution. Results are the average of four samples + standard error of the mean.

upon incubation with HepG2 cells at the highest tested concentration, 100 nM, for 2 and 24 h using the lactate dehydrogenase (LDH) leakage assay following established protocols [45,46]. Toxic interaction of cationic dendrimers with mammalian cells proved to destabilize the cell membrane and increase the leakage of LDH enzyme into the culture medium, which is used as a measure for particle toxicity compared to baseline LDH leakage observed under normal culture conditions [45,46]. Results show that all G5-based conjugates tested in this study produced insignificant LDH leakage compared to that observed upon incubation of HepG2 cells in regular culture medium for 2 and 24 h (Fig. 10), which indicates that these G5-NAcGal conjugates are nontoxic and can be used as drug carriers for targeted delivery into hepatic cancer cells.

4. Conclusions

We have successfully synthesized G5-NAcGal conjugates using two different coupling strategies, which allow tuning the number of NAcGal molecules attached per single G5 carrier. Cationic G5-(Fl)-$(NH_2)_{122}$ dendrimers showed similar internalization into both HepG2 and MCF-7 cells via adsorptive-mediated endocytosis, which is a fast and efficient internalization route but it fails to discriminate between different mammalian cells and should not be exploited for cell-specific drug delivery. Conjugation of 12 NAcGal molecules to G5 dendrimers yielded G5-NAcGal conjugates that were selectively internalized by almost 100% of hepatic cancer cells within a short period of time. The low number of NAcGal molecules required to trigger receptor-mediated endocytosis of G5-NAcGal conjugates into hepatic cancer cells leaves approximately 90% of the NH_2 surface groups available for loading of drug and imaging molecules, which expands the therapeutic utility of these carriers. Results clearly show that NAcGal-targeted G5 dendrimers present a highly efficient carrier for selective delivery of therapeutic molecules into the cytoplasm of hepatic cancer cells for a wide range of therapeutic applications.

Acknowledgments

This research is supported by the US National Science Foundation CAREER Award and Coulter Foundation Translational Research Partnership in Biomedical Engineering Award (to Mohamed El-Sayed). Scott Medina recognizes the financial support of the Department of Education GAANN Fellowship. We thank Dr. Michael Mayer for providing access to the Nikon Eclipse TE2000-U inverted microscope.

Appendix. Supplementary data

Supplementary data related to this article can be found online at doi:10.1016/j.biomaterials.2010.11.068.

References

[1] Tomalia DA, Baker H, Dewald J, Hall M, Kallos G, Martin S, et al. A new class of polymers: starburst-dendritic macromolecules. Polym J 1985;17:117.
[2] Patri AK, Majoros IJ, Baker JR. Dendritic polymer macromolecular carriers for drug delivery. Curr Opin Chem Biol 2002;6:466–71.
[3] Tomalia DA, Reyna LA, Svenson S. Dendrimers as multi-purpose nanodevices for oncology drug delivery and diagnostic imaging. Biochem Soc Trans 2007;035:61–7.
[4] Svenson S, Tomalia DA. Dendrimers in biomedical applications–reflections on the field. Adv Drug Deliv Rev 2005;57:2106–29.
[5] Kobayashi H, Brechbiel MW. Nano-sized MRI contrast agents with dendrimer cores. Adv Drug Deliv Rev 2005;57:2271.
[6] Kobayashi H, Kawamoto S, Jo S-K, Bryant HL, Brechbiel MW, Star RA. Macromolecular MRI contrast agents with small dendrimers: pharmacokinetic differences between sizes and cores. Bioconjug Chem 2003;14:388–94.
[7] Zhou J, Wu J, Hafdi N, Behr J-P, Erbacher P, Peng L. PAMAM dendrimers for efficient siRNA delivery and potent gene silencing. Chem Commun 2006: 2362–4.
[8] Zhong H, He Z-G, Li Zheng, Li G-Y, Shen S-R, Li X-L. Studies on polyamidoamine dendrimers as efficient gene delivery vector. J Biomater Appl 2008;22:527–44.
[9] Navarro G, Tros de Ilarduya C. Activated and non-activated PAMAM dendrimers for gene delivery in vitro and in vivo. Nanomedicine: NBM 2009;5: 287–97.
[10] Medina SH, El-Sayed MEH. Dendrimers as carriers for delivery of chemotherapeutic agents. Chem Rev 2009;109:3141–57.
[11] Patri AK, Myc A, Beals J, Thomas TP, Bander NH, Baker JR. Synthesis and *in vitro* testing of J591 antibody–dendrimer conjugates for targeted prostate cancer therapy. Bioconjug Chem 2004;15:1174–81.
[12] Shukla R, Thomas TP, Peters JL, Desai AM, Kukowska-Latallo J, Patri AK, et al. HER2 specific tumor targeting with dendrimer conjugated anti-HER2 mAb. Bioconjug Chem 2006;17:1109–15.
[13] Sato N, Kobayashi H, Hiraga A, Saga T, Togashi K, Konishi J, et al. Pharmacokinetics and enhancement patterns of macromolecular MR contrast agents with various sizes of polyamidoamine dendrimer cores. Magn Reson Med 2001;46:1169–73.
[14] Kukowska-Latallo JF, Candido KA, Cao Z, Nigavekar SS, Majoros IJ, Thomas TP, et al. Nanoparticle targeting of anticancer drug improves therapeutic response in animal model of human epithelial cancer. Cancer Res 2005;65: 5317–24.
[15] Shi X, Wang SH, Swanson SD, Ge S, Cao Z, Van Antwerp ME, et al. Dendrimer-functionalized shell-crosslinked iron oxide nanoparticles for *in-vivo* magnetic resonance imaging of tumors. Adv Mater 2008;20:1671–8.
[16] Swanson SD, Kukowska-Latallo JF, Patri AK, Chen C, Ge S, Cao Z, et al. Targeted gadolinium-loaded dendrimer nanoparticles for tumor-specific magnetic resonance contrast enhancement. Int J Nanomedicine 2008;3:201–10.
[17] Backer MV, Gaynutdinov TI, Patel V, Bandyopadhyaya AK, Thirumamagal BTS, Tjarks W, et al. Vascular endothelial growth factor selectively targets boronated dendrimers to tumor vasculature. Mol Cancer Ther 2005;4: 1423–9.
[18] Schwartz AL, Fridovich SE, Knowles BB, Lodish HF. Characterization of the asialoglycoprotein receptor in a continuous hepatoma line. J Biol Chem 1981; 256:8878–81.
[19] Jain V, Nath B, Gupta GK, Shah PP, Siddiqui MA, Pant AB, et al. Galactose-grafted chylomicron-mimicking emulsion: evaluation of specificity against HepG-2 and MCF-7 cell lines. J Pharm Pharmacol 2009;61: 303–10.
[20] David A, Kopeckova P, Rubinstein A, Kopecek J. Enhanced biorecognition and internalization of HPMA copolymers containing multiple or multivalent carbohydrate side-chains by human hepatocarcinoma cells. Bioconjug Chem 2001;12:890–9.
[21] Seymour LW, Ferry DR, Anderson D, Hesslewood S, Julyan PJ, Poyner R, et al. Hepatic drug targeting: phase I evaluation of polymer-bound doxorubicin. J Clin Oncol 2002;20:1668–76.
[22] Liang H-F, Yang T-F, Huang C-T, Chen M-C, Sung H-W. Preparation of nanoparticles composed of poly(gamma-glutamic acid)-poly(lactide) block copolymers and evaluation of their uptake by HepG2 cells. J Control Release 2005; 105:213–25.
[23] Liang H-F, Chen S-C, Chen M-C, Lee P-W, Chen C-T, Sung H-W. Paclitaxel-loaded poly(gamma-glutamic acid)-poly(lactide) nanoparticles as a targeted drug delivery system against cultured HepG2 cells. Bioconjug Chem 2006;17: 291–9.
[24] El-Sayed M, Kiani MF, Naimark MD, Hikal AH, Ghandehari H. Extravasation of poly(amidoamine) (PAMAM) dendrimers across microvascular network endothelium. Pharm Res 2001;18:23–8.
[25] Quintana A, Raczka E, Piehler L, Lee I, Myc A, Majoros I, et al. Design and function of a dendrimer-based therapeutic nanodevice targeted to tumor cells through the folate receptor. Pharm Res 2002;19:1310–6.
[26] Albertazzi L, Serresi M, Albanese A, Beltram F. Dendrimer internalization and intracellular trafficking in living cells. Mol Pharmacol 2010;7:680–8.
[27] Kitchens KM, Kolhatkar RB, Swaan PW, Ghandehari H. Endocytosis inhibitors prevent poly(amidoamine) dendrimer internalization and permeability across Caco-2 cells. Mol Pharmacol 2008;5:364–9.
[28] Kitchens K, Foraker A, Kolhatkar R, Swaan P, Ghandehari H. Endocytosis and interaction of poly (amidoamine) dendrimers with Caco-2 cells. Pharm Res 2007;24:2138–45.
[29] Kitchens K, El-Sayed MEH, Ghandehari H. Transepithelial and endothelial transport of poly(amidoamine) dendrimers. Adv Drug Deliv Rev 2005;57: 2163–76.
[30] Kitchens K, Kolhatkar R, Swaan P, Eddington N, Ghandehari H. Transport of poly(amidoamine) dendrimers across Caco-2 cell monolayers: influence of size, charge and fluorescent labeling. Pharm Res 2006;23:2818–26.
[31] Kolhe P, Khandare J, Pillai O, Kannan S, Lieh-Lai M, Kannan RM. Preparation, cellular transport, and activity of polyamidoamine-based dendritic nanodevices with a high drug payload. Biomaterials 2006;27:660–9.
[32] Dong Q, Hurst DR, Weinmann HJ, Chenevert TL, Londy FJ, Prince MR. Magnetic resonance angiography with gadomer-17. An animal study original investigation. Invest Radiol 1998;33:699–708.
[33] Kobayashi H, Kawamoto S, Saga T, Sato N, Hiraga A, Konishi J, et al. Micro-MR angiography of normal and intratumoral vessels in mice using dedicated intravascular MR contrast agents with high generation of polyamidoamine

dendrimer core: reference to pharmacokinetic properties of dendrimer-based MR contrast agents. J Magn Reson Imaging 2001;14:705–13.
[34] McKendry R, Huck WTS, Weeks B, Fiorini M, Abell C, Rayment T. Creating nanoscale patterns of dendrimers on silicon surfaces with dip-pen nanolithography. Nano Lett 2002;2:713–6.
[35] Gabellieri E, Strambini GB, Shcharbin D, Klajnert B, Bryszewska M. Dendrimer–protein interactions studied by tryptophan room temperature phosphorescence. Biochim Biophys Acta 2006;1764:1750–6.
[36] Cakara D, Kleimann J, Borkovec M. Microscopic protonation equilibria of poly (amidoamine) dendrimers from macroscopic titrations. Macromolecules 2003;36:4201–7.
[37] Diallo M, Christie S, Swaminathan P, Johnson J, Goddard W. Dendrimer enhanced ultrafiltration. 1. Recovery of Cu(II) from aqueous solutions using PAMAM dendrimers with ethylene diamine core and terminal NH_2 groups. Environ Sci Technol 2005;39:1366–77.
[38] Lloyd JB, Duncan R, Kopecek J. Synthetic polymers as targetable carriers for drugs. Pure Appl Chem 1984;56:1301–4.
[39] Perumal OP, Inapagolla R, Kannan S, Kannan RM. The effect of surface functionality on cellular trafficking of dendrimers. Biomaterials 2008;29:3469–76.
[40] Seib FP, Jones AT, Duncan R. Comparison of the endocytic properties of linear and branched PEIs, and cationic PAMAM dendrimers in B16f10 melanoma cells. J Control Release 2007;117:291–300.
[41] Hillaireau H, Couvreur P. Nanocarriers' entry into the cell: relevance to drug delivery. Cell Mol Life Sci 2009;66:2873–96.
[42] Behr J-P. The proton sponge: a trick to enter cells the viruses did not exploit. Chimia 1997;51:34–6.
[43] Kono K, Akiyama H, Takahashi T, Takagishi T, Harada A. Transfection activity of polyamidoamine dendrimers having hydrophobic amino acid residues in the periphery. Bioconjug Chem 2004;16:208–14.
[44] Schwartz AL, Fridovich SE, Lodish HF. Kinetics of internalization and recylcing of the asialoglycoprotein receptor in a hepatoma cell line. J Biol Chem 1982;257:4230–7.
[45] El-Sayed M, Ginski M, Rhodes C, Ghandehari H. Transepithelial transport of poly (amidoamine) dendrimers across Caco-2 cell monolayers. J Control Release 2002;81:355–65.
[46] El-Sayed M, Ginski M, Rhodes C, Ghandehari H. Influence of surface chemistry of poly (amidoamine) dendrimers on Caco-2 cell monolayers. J Bioact Compat Polym 2003;18:7–22.